Mechanism of Proton Insertion and Characterization of the Proton Sites in Lithium Manganate Spinels

Brett Ammundsen,† Deborah J. Jones, and Jacques Rozière*

Laboratoire des Agrégats Moléculaires et Matériaux Inorganiques, URA CNRS 79, Université Montpellier 2, Place Eugène Bataillon, 34095 Montpellier Cédex 5, France

Gary R. Burns*

Department of Chemistry, Victoria University of Wellington, PO Box 600, Wellington, New Zealand

Received May 25, 1995. Revised Manuscript Received September 5, 1995®

Protonated forms of the spinel manganese dioxide phase λ-MnO_2 have been prepared by the ion-exchange of three different lithium manganate precursors. The mechanisms of lithium extraction and proton insertion were examined in each case by X-ray diffraction and chemical and thermal analyses. The amount of protons inserted by ion exchange differed according to the composition of the precursor lithium manganate, the distribution of cations between 8a tetrahedral and 16d octahedral sites, and the oxidation state of the manganese, all of which depend on the method of preparation. The proton sites in the λ-MnO_2 materials were characterized using a combination of inelastic neutron scattering (INS) and infrared spectroscopies. The strongest features in the INS spectra, at 910 and 1080 cm^{-1}, are assigned to OH deformation modes. These results are discussed in relation to thermal analysis and infrared data for the manganese dioxides pyrolusite (β-MnO_2) and synthetic ramsdellite, and the proton sites explained using a conventional model for the manganese oxide lattice. The 910 cm^{-1} mode dominated the INS spectra of all three λ-MnO_2 materials and is assigned to lattice hydroxyl groups associated with the vacant 8a tetrahedral sites in the structure. The presence of an INS mode at 1080 cm^{-1} was observed for only one of the λ-MnO_2 samples and is attributed to protons in interstitial sites, associated with a small amount of Mn^{III} in the material. Variable temperature infrared spectroscopy and X-ray diffraction showed that the loss of water above 100 °C results in destruction of the λ-MnO_2 spinel lattice and suggests that water plays an important role in stabilizing the protonated λ-MnO_2 structure. A model is proposed in which protons associated with oxygen atoms at 16d octahedral vacancies form lattice water species.

Introduction

Lithium manganates, with structures that range from cubic through distorted spinel to rock salt, provide electrochemical materials of potential as cathodes for lithium batteries,[1–8] analytical materials in the form of lithium ion exchangers[9–14] and lithium ion sensors,[15] and catalysts for methane coupling.[16] Key reactions in all of these applications are proton and lithium ion insertion, and redox processes involving manganese.

Single-phase lithium manganates having the spinel structure have been prepared with lithium:manganese stoichiometries ranging from 1:2 to 4:5.[17] The extraction of lithium from these compounds, at low pH and at room temperature, produces the spinel phase of manganese dioxide, λ-MnO_2. For $LiMn_2O_4$ crystallized at a temperature of around 800 °C, the lithium extraction reaction has been shown[13,18,19] to be predominantly a redox reaction involving the oxidation of the Mn^{III} to Mn^{IV}. However, a different process involving ion exchange with protons has also been proposed for lithium

† On leave from the Department of Chemistry, Victoria University of Wellington.

® Abstract published in *Advance ACS Abstracts,* October 15, 1995.

(1) Goodenough, J. B.; Thackeray, M. M.; David, W. I. F.; Bruce, P. G. *Rev. Chim. Miner.* **1984**, *21*, 435.
(2) Thackeray, M. M.; de Kock, A.; Rossouw, M. H.; Liles, D. C.; Bittihn, R.; Hoge, D. *J. Electrochem. Soc.* **1992**, *139*, 363.
(3) Ohzuku, T.; Kitigawa, M.; Hirai, T. *J. Electrochem. Soc.* **1990**, *137*, 40.
(4) Ohzuku, T.; Kato, M. J.; Sawai, K.; Hirai, T. *J. Electrochem. Soc.* **1991**,*138*, 2556.
(5) Li, L.; Pistoia, G. *Solid State Ionics* **1991**, *47*, 231, 241.
(6) Lubin, F.; Lecerf, A.; Broussely, M.; Labat, J. *J. Power Sources* **1991**, *34*, 161.
(7) Guyomard, D.; Tarascon, J. M. *J. Electrochem. Soc.* **1992**, *139*, 937.
(8) Shokoohi, F. K.; Tarascon, J. M.; Wilkens, B. J.; Guyomard, D.; Chang, C. C. *J. Electrochem. Soc.* **1992**, *139*, 937.
(9) Vol'khin, V. V.; Leont'eva, G. V.; Onolin, S. A. *Neorg. Mater.* **1973**, *6*, 1041.
(10) Leont'eva, G. V.; Chirkova, L. G. *Zh. Prikl. Khim.* **1988**, *61*, 734.
(11) Shen, X.-M.; Clearfield, A. J. *J. Solid State Chem.* **1986**, *64*, 270.
(12) Ooi, K.; Miyai, Y.; Katoh, S.; Maeda, H.; Abe, M. *Langmuir* **1989**, *5*, 150.
(13) Ooi, K.; Miyai, Y.; Katoh, S.; Maeda, H.; Abe, M. *Langmuir* **1990**, *6*, 289 and references therein.
(14) Burns, G. R.; Kane, C.; Sahasrabudhe, N. In *New Developments In Ion Exchange*; Abe, M., Kataoka, T., Suzuki, T., Eds.; Kodansha and Elsevier: Tokyo, Amsterdam, 1991; p 523.
(15) Kanoh, H.; Feng, Q., Miyai, Y.; Ooi, K. *J. Electrochem. Soc.* **1993**, *140*, 3162.
(16) Aitchison, P. B.; Burns, G. R.; Patterson, J. *J. Catal.*, submitted.
(17) Thackeray, M. M.; de Kock, A.; David, W. I. F. *Mater. Res. Bull.* **1993**, *28*, 1041.
(18) Hunter, J. C. *J. Solid State Chem.* **1981**, *39*, 142.
(19) Feng, Q.; Miyai, Y.; Kanoh, H.; Ooi, K. *Langmuir* **1992**, *8*, 1861.

0897-4756/95/2807-2151$09.00/0

manganates prepared at lower temperature[10,11] and with higher lithium:manganese ratios.[19]

The lithium ion extraction process has been studied by ^{6}Li and ^{7}Li MAS NMR spectroscopy,[20] and the Li sites characterized for both the mixed manganese valence state spinel $LiMn^{III}Mn^{IV}O_4$ and the single manganese valence state spinel $Li_4Mn^{IV}_5O_{12}$, as well as for the rock salt lithium manganate Li_2MnO_3. X-ray absorption spectra of $LiMn_2O_4$ and $Li_4Mn_5O_{12}$[21] have enabled changes in oxidation state associated with the extraction and reinsertion of lithium ions to be followed for these two spinels and confirmed the presence of both Mn^{III} and Mn^{IV} in $LiMn_2O_4$ and the predominance of Mn^{IV} in $Li_4Mn_5O_{12}$ and in the λ-MnO_2 phases derived by acid-washing both parent compounds. These results support the suggestion that lithium extraction from and reinsertion into spinels must occur by different mechanisms according to the quantity of Mn^{III} present in the original lithium manganates.

While the techniques so far applied to determining the structural characteristics and dynamic properties of lithium manganates have aided our understanding of lithium extraction and insertion, there has been, to our knowledge, no detailed study of the proton insertion process and, to some extent, the presence of lattice protons has been ignored or remained undetected in some of the cited studies. Clearly, in order to better understand the insertion and deinsertion of lithium ions, the dynamics of the proton exchange process and the nature of the proton sites must be clarified.

The types of possible proton site in λ-MnO_2, the lithium deinserted phase of the lithium manganate spinels, should be related to the proton sites in other manganese oxide phases, particularly the various forms of γ-MnO_2, which is described as a structure composed of intergrowths of pyrolusite (β-MnO_2) and ramsdellite. From a series of spectroscopic investigations of proton insertion in γ-MnO_2,[22-24] it was concluded that the protons which can be removed by thermal treatment up to 450 °C are not covalently bound to oxygen atoms. The principal features in the INS spectra of variously prepared samples of γ-MnO_2 were attributed to protons trapped in sites defined by an environment of oxygen octahedra, similar to the proton sites in metal hydrides. The chemical consequences of hydrogen being nonbonded to lattice oxygen in these materials raises some major questions for the current models of chemical bonding of hydrogen in manganese oxides.

The objectives of this study are therefore 3-fold. First, to investigate the ion-exchange reactions for a series of lithium manganate spinel materials prepared under similar conditions but from different starting compounds and to verify the relationships between proton insertion and manganese oxidation state. Second, to use infrared and incoherent inelastic neutron scattering spectroscopy to obtain data on the phonons and vibrational modes associated with inserted protons in λ-MnO_2 phases and to compare these data with those obtained for the manganese dioxides pyrolusite and synthetic ramsdellite. Finally, we wished to test the validity of a conventional model for the protons in manganese dioxide materials, based on the presence of hydroxyl groups with binding energies that are largely determined by the geometry of the nearest neighbor lattice oxygens.

Experimental Section

Three different methods were used to attempt to prepare samples of lithium manganate with the stoichiometry $Li_4Mn_5O_{12}$. In one case (preparation C) the finely ground precursors, lithium carbonate and manganese carbonate, in a molar ratio of 0.8, were fired at 400 °C for 4 h in air. The second preparation (G), involved using a 0.8 molar ratio of lithium nitrate and γ-MnO_2, finely ground and fired at 400 °C for 20 h. The third preparation (P) used lithium nitrate and pyrolusite (β-MnO_2) in a 0.8 ratio. The finely ground mixture was again fired at 400 °C for 20 h with a flow of air maintained over the sample.

Lithium extraction reactions for the lithium manganates (C), (G), and (P) were achieved by stirring samples in 0.2 M solutions of hydrochloric acid for 48 h at room temperature, followed by drying at 60 °C. The products obtained from each of the parent lithium manganates are denoted λ-MnO_2(C), λ-MnO_2(G), and λ-MnO_2(P).

Samples of the three lithium manganate precursors and of the three acid-treated samples were dissolved with mixed solutions of HCl and H_2O_2 and analyzed for lithium and manganese content by atomic emission spectrometry.

Reinsertion of lithium in the λ-MnO_2 materials was achieved by stirring samples in 0.1 M solutions of lithium chloride for 72 h at room temperature, followed by drying at 60 °C.

Synthetic ramsdellite was prepared by heating $LiMn_2O_4$ with 2.5 M sulphuric acid at 90 °C for 24 h, following the method first described by Kondrasev and Zaslavskij[25] and more recently by Rossouw et al.[26] The $LiMn_2O_4$ used as the starting material was synthesized by firing a 1:2 molar ratio of lithium carbonate and manganese carbonate in at 800 °C for 20 h in air. The ramsdellite obtained by this preparation has since been shown to contain a portion of de Wolff defects (i.e., pyrolusite domains) and could therefore be better described as having a γ-MnO_2 structure.[27] However to avoid ambiguity, we will continue to refer to this sample as "synthetic ramsdellite" in the discussion which follows.

The pyrolusite sample was prepared by heating β-MnO_2 (99.5% purity, Aldrich) in nitric acid at 100 °C for 5 h.[5]

Infrared data between 25 and 220 °C were measured under dynamic vacuum on samples dispersed in KBr using a VLT2 cell mounted in a Bomem DA8 FTIR spectrometer.

Incoherent inelastic neutron scattering (INS) spectra were recorded on the TFXA spectrometer at the spallation neutron source ISIS (Rutherford Appleton Laboratory), on samples contained in thin-walled aluminum holders 5 × 2 cm^2. Data were collected at 26 K for ca. 2000 μA h and were processed using RAL routines.

Thermal gravimetry (TG) and differential thermal analysis (DTA) data were obtained in air using an automated Stanton Redcroft STA-781 series thermal analyzer at a heating rate of 2 °C/min.

X-ray diffraction (XRD) powder patterns were recorded by multiply scanning on an automated Phillips diffractometer using Cu Kα radiation. In the variable temperature studies, samples were heated in increments of 20 °C and stabilized at

(20) Morgan, K. R.; Burns, G. R.; Collier, S. J.; Ooi, K. *J. Chem. Soc., Chem. Commun.* **1994**, 1719.
(21) Ammundsen, B.; Burns, G. R.; Jones, D. J.; Rozière, J. *Proceedings of the International Conference on Ion Exchange 1995*, submitted.
(22) Fillaux, F.; Ouboumour, H.; Tomkinson, J.; Yu, L. T. *Chem. Phys.* **1991**, *149*, 459.
(23) Fillaux, F.; Ouboumour, H.; Cachet, C. H.; Kearley, G. J.; Tomkinson, J.; Yu, L. T. *Physica B* **1992**, *180, 181*, 680.
(24) Fillaux, F.; Ouboumour, H.; Cachet, C. H.; Tomkinson, J.; Levy-Clement, C.; Yu, L. T. *J. Electrochem. Soc.* **1993**, *140*, 585, 592.
(25) Kondrasev, J. D.; Zaslavskij, A. I. *Isv. Akad. Nauk SSSR Fiz.* **1951**, *15*, 179.
(26) Rossouw, M. H.; de Kock, A.; Liles, D. C.; Gummow, R. J.; Thackeray, M. M. *J. Mater. Chem.* **1992**, *2*, 1211.
(27) Pannetier, J.; Chabre, Y. *Prog. Solid State Chem.*, in press.

Table 1. Compositional and Structural Parameters for the Spinel Lithium Manganates

sample	a_0 (Å)	Li/Mn	x^a	y^a	formula	cation distribution
(C)	8.15	0.787	0.32	0	$Li_{1.32}Mn_{1.68}O_4$	$(Li)[Li_{0.32}Mn^{III}_{0.04}Mn^{IV}_{1.64}]O_4$
(G)	8.14	0.796	0.33	0	$Li_{1.33}Mn_{1.67}O_4$	$(Li)[Li_{0.33}Mn^{IV}_{1.67}]O_4$
(P)	8.20	0.507	0.01	0.24	$Li_{1.01}Mn_{1.99}O_{4.12}$	$(Li_{0.97}\square_{0.03})[Li_{0.01}\square_{0.06}Mn^{III}_{0.71}Mn^{IV}_{1.22}]O_4$

[a] In $Li_{(1+x)}Mn^{III}_{(1-3x-y)}Mn^{IV}_{(1+2x+y)}O_{(4+0.5y)}$.

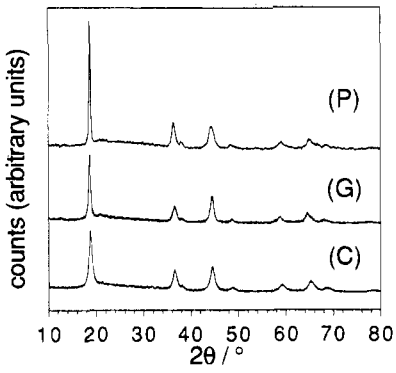

Figure 1. XRD patterns for the lithium manganate materials prepared by the three different methods (C), (G), and (P) (see text).

each temperature for 2–3 h during the collection of the XRD pattern by multiple scans.

Results and Discussion

Discussion of the experimental results is presented in two sections. In section I we report the compositions and structures of the lithium manganates and of the derived λ-MnO_2 spinels as determined from elemental, X-ray, and DTA-TG analyses and summarize the implications of these results in terms of the mechanism of proton insertion for these materials. In section II we report IR and INS spectroscopic data for the protonated λ-MnO_2 samples and discuss in more depth the characteristics of the proton sites in the spinel lattice. Comparative data for the manganese dioxides pyrolusite and synthetic ramsdellite are presented at each stage.

I. Elemental, X-ray, and DTA-TG Analyses. *Structure and Composition of the Lithium Manganates.* The XRD patterns for the three lithium manganate preparations (C), (G), and (P), shown in Figure 1, confirmed that all three materials were composed of a single cubic spinel phase. Sharper lines were found for the preparation from pyrolusite, indicating that this material was more crystalline than those obtained from carbonates or from γ-MnO_2. The (P) preparation also had a higher unit cell parameter of 8.20 Å, compared with 8.15 and 8.14 Å for the other two spinels (C) and (G), respectively. A lowering of the unit cell parameter of spinel lithium manganates, which may vary from 8.24 Å to as low as 8.14 Å,[17] is related to an increase in the mean oxidation state of the manganese. An increase in the proportion of Mn^{IV} relative to Mn^{III} is associated with vacancies in 16d octahedral sites or occupation of a proportion of these sites by lithium. The difference in lattice parameter between that of the lithium manganate (P) and that of the preparations (C) and (G) is a first indication that the mean oxidation state of the manganese was lower in the (P) material, i.e., that it contained a greater amount of Mn^{III}.

Elemental analysis for lithium and manganese content also showed differences between the three materials. The found Li:Mn molar ratios are given in Table 1. Although a Li:Mn starting ratio of 0.8 was effectively retained in the spinels (C) and (G), the spinel (P) was found to have a Li:Mn ratio of only 0.51, implying the loss of nearly a third of the lithium in the reaction. This result is surprising, but has been observed in other studies where it has been attributed to evaporation of $LiNO_3$,[5] in this case probably facilitated by passing a flow of air over the sample during calcination.

The spinel structure belongs to the space group *Fd3m*. Single phase spinel lithium manganates may be prepared with Li:Mn stoichiometries ranging between 0.5 and 0.8 to give compositions with the formula $Li_{1+x}Mn_{2-x}O_4$, where $0 < x < 0.33$. When $x = 0$, giving the spinel $LiMn_2O_4$, lithium ions are located in tetrahedral 8a sites and manganese in octahedral 16d sites. The distribution of lithium and manganese ions between tetrahedral and octahedral sites has recently been determined for compositions where $x > 0$, based on neutron diffraction data.[17] As x approaches a maximum value of 0.33, giving the composition $Li_{1.33}Mn_{1.67}O_4$, neutron diffraction data demonstrate that there are a small number of vacancies on the tetrahedral 8a sites but that the octahedral 16d sites are completely filled with manganese and lithium. The cation distribution when $x = 0.33$ may therefore be expressed in "spinel notation" as $(Li)[Li_{0.33}Mn_{1.67}]O_4$, where the cations written in round brackets and in square brackets are those in the tetrahedral and octahedral sites, respectively. The Li:Mn stoichiometries found for the spinels (C) and (G) establish values of 0.32 and 0.33, respectively, for x in these compounds. The Li:Mn ratio found for the spinel (P) however gives only a small value of $x = 0.01$. It may be that the high crystallinity of the pyrolusite lithiated in the reaction, which gives rise to a more crystalline spinel than does the reaction with the poorly crystalline γ-MnO_2 or does the reaction between carbonate salts, limits the amount of lithium that can be introduced into octahedral sites in the derived spinel structure.

Lithium manganate spinels with $x > 0$ are metastable, and above 400 °C form a mixture of the stable spinel $LiMn_2O_4$ and the rock salt phase Li_2MnO_3. This transformation is accompanied by a loss of oxygen associated with the reduction of a certain portion of "excess" Mn^{IV} present in the low-temperature spinel as a result of the higher Li:Mn ratio. The low temperature of preparation (up to 400 °C) may further give an increase in the proportion of Mn^{IV} relative to Mn^{III} due to the presence of unoccupied cation sites. These vacancies are statistically distributed across both 8a and 16d sites[28] and give an "oxygen-rich" spinel with a corresponding stoichiometric increase in Mn^{IV}. The loss of the vacancies above 400 °C is therefore also accompanied by the loss of oxygen and reduction of a proportion of Mn^{IV}. The expected weight loss can be related to the value of x (representing lithium stoichi-

(28) de Kock, A.; Rossouw, M. H.; de Picciotto, L. A.; Thackeray, M. M.; David, W. I. F.; Ibberson, R. M. *Mater. Res. Bull.* **1990**, *25*, 657.

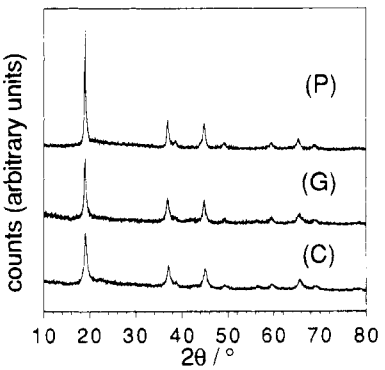

Figure 2. XRD patterns for λ-MnO_2 materials derived by acid-washing the three different lithium manganate precursors (C), (G), and (P) (see text).

ometry in excess of 1) in the original compound, and to a second parameter y, which represents the increase in Mn^{IV} due to cation vacancies, according to the process:

$$Li_{(1+x)}Mn^{III}_{(1-3x-y)}Mn^{IV}_{(1-2x+y)}O_{(4+0.5y)} \xrightarrow{-(0.5x+0.25y)O_2} (1-x)LiMn^{III}Mn^{IV}O_4 + xLi_2Mn^{IV}O_3$$

where $0 < y < 1 - 3x$. Because x is determined from a chemical analysis, the value for y can be evaluated from the total observed weight loss.

Thermogravimetric analyses of the weight loss between 400 and 800 °C for the lithium manganates (C) and (G) were consistent with a value of $y = 0$ for these compounds, as expected when x has a value close to 0.33. A much smaller weight loss was observed in this temperature range for the lithium manganate (P). The analysis gave a value of $y = 0.24$, and the relative proportions of Mn^{III} and Mn^{IV} in the material (P) were therefore evaluated on the basis of a small number of cation vacancies in the structure.

The compositional and structural parameters, derived from the chemical, thermogravimetric, and XRD analyses, are summarized in Table 1 for the three lithium manganates. Also given are the calculated formulas, and the derived cation distributions assuming that vacancies due to excess oxygen are distributed across 8a and 16d sites in a 1:2 ratio and that "excess" lithium is present in octahedral 16d sites.

Structure and Composition of the Lithium-Extracted Spinels. Lithium extraction reactions were carried out for each of the three lithium manganate spinels in aqueous acid under identical conditions to give the corresponding λ-MnO_2 materials. The XRD patterns for λ-MnO_2(C), λ-MnO_2(G), and λ-MnO_2(P) (Figure 2) show that the diffraction lines of the spinel structure remain after acid treatment but are shifted to slightly higher 2θ values. The lithium extraction reaction proceeds topotactically with a decrease in the lattice constant relating to the amount of lithium extracted.[2,18] The unit-cell parameters for the three lithium-extracted λ-MnO_2 materials were found to vary consistently with the extent of lithium extraction achieved. A residual lithium content of 0.015 mol/mol of manganese was found for λ-MnO_2(C), showing that 97% extraction of lithium had occurred by the acid treatment of the parent lithium manganate. The resulting spinel had a unit-cell parameter of 8.04 Å. Effectively no lithium was found in λ-MnO_2(G), which had a unit-cell parameter of 8.03 Å, from which it may be concluded that the lithium was almost completely extracted from the precursor. However, the λ-MnO_2(P) preparation was found to contain 0.10 mol of lithium/mol of manganese, corresponding to extraction of only 81% of the lithium from the parent spinel. λ-MnO2(P) had the highest unit cell parameter of 8.06 Å.

Studies of the extraction of lithium from lithium manganate spinels suggest that two different reactions may be involved.[19] For the spinel $LiMn_2O_4$, which contains equal amounts of Mn^{III} and Mn^{IV}, lithium extraction is expected to occur mainly by a redox process:

$$4LiMn^{III}Mn^{IV}O_4 + 8H^+ \rightarrow 3Mn^{IV}{}_2O_4 + 4Li^+ + 2Mn^{2+} + 4H_2O \quad (1)$$

However, at a maximum Li:Mn stoichiometry of 0.8, giving the spinel $Li_{1.33}Mn_{1.67}O_4$, all the manganese is in oxidation state IV, and lithium extraction should occur by an ion-exchange process to give a protonated λ-MnO_2:

$$3Li_{1.33}Mn^{IV}{}_{1.67}O_4 + 4H^+ \rightarrow 3H_{1.33}Mn^{IV}{}_{1.67}O_4 + 4Li^+ \quad (2)$$

At intermediate compositions both reactions occur, the extent of proton insertion depending on the relative proportions of Mn^{III} and Mn^{IV} in the parent spinel. These relationships have been discussed in detail by Feng et al.[19] The amount of proton inserted on the extraction of lithium is directly related to both the amount of octahedral lithium and the number of 16d octahedral vacancies in the parent structures, and may therefore be calculated from the parameters x and y (given in Table 1). The stoichiometric amount of proton inserted per lithium ion extracted is given by

$$H^+ \text{ inserted/} Li^+ \text{ extracted} = (4x + y)/(1 + x)$$

Applying these relationships to the spinels (C) and (G), which had manganese mean oxidation states very close to 4.0, lithium extraction is expected to occur with insertion of greater than 0.95 equiv of H^+. However, up to a third of the protons inserted during the initial lithium extraction are not reexchangeable for lithium in 0.1 M LiOH solution.[19] Additional proof that the extraction–reinsertion process involves no detectable change in manganese oxidation state has been provided by X-ray absorption spectroscopy.[21]

On the other hand, in the spinel (P) the higher Mn^{III}/Mn^{IV} ratio results in a greater contribution of a redox process to lithium extraction, and consequently a much lower proton content is expected in λ-MnO_2(P).

Higher proton contents for λ-MnO_2(C) and λ-MnO_2-(G) compared to λ-MnO_2(P) are supported by thermogravimetric analysis. It has been proposed[19] that an approximate evaluation of the lattice proton content of a spinel λ-MnO_2 material can be made from the weight loss up to 300 °C, as in this temperature range a dissipation of water by the condensation of lattice hydroxyl groups is expected to occur. The thermogravimetric curves for the three samples of λ-MnO_2 together with the corresponding DTA data are given in Figure 3 and show a significantly greater weight loss up to 300

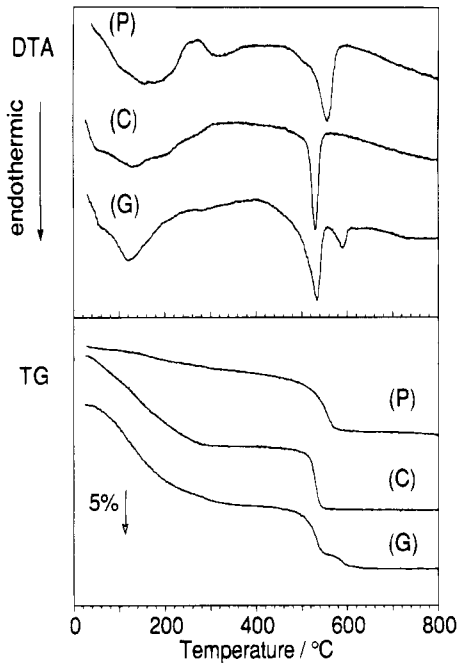

Figure 3. DTA and TG curves for λ-MnO_2 (P), (C), and (G).

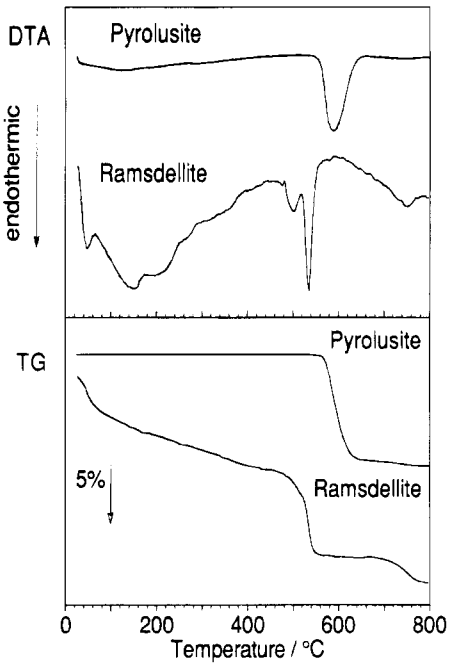

Figure 4. DTA and TG curves for pyrolusite and synthetic ramsdellite.

°C for λ-MnO_2(C) and λ-MnO_2(G) than for λ-MnO_2(P). It is also notable that for both the (C) and (G) λ-MnO_2 materials there is almost no loss in mass beyond 300 °C and before the beginning of the loss of oxygen at around 500 °C, which accompanies the transformation of the manganese dioxides to the sesquioxide Mn_2O_3. For λ-MnO_2 (P), however, there is a continuous loss of mass above 300 °C up to the transformation to Mn_2O_3.

All three λ-MnO_2 materials showed a weight loss between 500 and 600 °C in the reduction to Mn_2O_3, but the TG curves and the corresponding endotherms in the DTA data differed between samples. For λ-MnO_2(C), a sharp transformation was observed at 530 °C. In the case of λ-MnO_2(G) the reduction apparently occurred in two steps, with the main transition at 530 °C followed by a second smaller endothermic event at 590 °C. The relative broadening of the DTA endotherm for λ-MnO_2-(P), and the position of its maximum at 560 °C, higher in temperature compared to the main transitions observed for the other two λ-MnO_2 materials, may be partly explained by the higher amount of residual lithium in this material, giving rise to the formation of $LiMn_2O_4$ phase with Mn_2O_3. The differences may also be related to different manganese oxidation states in the samples. A significant amount of residual lithium in λ-MnO_2(P) implies that some Mn^{III} remains in the material. If lithium extraction occurred with insertion of the predicted 0.28 equiv of protons, around 8% of the total manganese in λ-MnO_2(P) would have remained as Mn^{III}. This result is important in regard to the spectroscopic observations discussed in section II of this paper.

Compositional and structural data for the three λ-MnO_2 materials are summarized in Table 2. Although the chemical formula for each sample has been calculated assuming that exchange for lithium ions has taken place up to the full capacity determined by the composition of the parent compound, assignment to specific sites in the structure is not attempted at this stage for either protons or residual lithium.

Pyrolusite and Synthetic Ramsdellite. Thermal analyses of samples of pyrolusite and synthetic ramsdellite were carried out to measure data comparative to that for the λ-MnO_2 materials. The DTA and TG results are shown in Figure 4. Pyrolusite shows no discernible weight loss until the transformation to Mn_2O_3 occurs at 600 °C, with the expected 9% loss in mass. Synthetic ramsdellite, however, displays a weight loss of 6.9% up to 400 °C with a matching broad endotherm in the DTA data. The feature in the endotherm at approximately 150 °C coincides with the complete loss in infrared spectroscopy (see below) of absorption bands attributable to water. The 3.9% loss in mass up to 150 °C then leaves as a minimum 3% of the mass as being attributable to the loss of lattice hydroxyl groups. The transformation to Mn_2O_3 in the synthetic ramsdellite is then accompanied by a weak endotherm at 500 °C and major endotherm at 530 °C.

The TG and DTA data for synthetic ramsdellite and pyrolusite are related to differences in their crystal structures. The pyrolusite was highly crystalline and expected to have a mean oxidation state of manganese very close to 4.0. The synthetic ramsdellite sample was of relatively lower crystallinity, and the differences observed in the thermal analysis are attributed to the progressive loss of water and condensation of lattice hydroxyl groups associated with both Mn^{IV} vacancies

Table 2. Compositional and Structural Parameters for the Lithium-Extracted Spinels

sample	precursor (from Table 1)	a_0 (Å)	Li/Mn	$H^+_{inserted}/Li_{extracted}$ (calculated)	formula
λ-MnO_2(C)	$Li_{1.32}Mn_{1.68}O_4$	8.04	0.015	0.97	$Li_{0.03}H_{1.25}Mn^{IV}_{1.68}O_4$
λ-MnO_2(G)	$Li_{1.33}Mn_{1.67}O_4$	8.03	0.005	0.99	$Li_{0.01}H_{1.31}Mn^{IV}_{1.67}O_4$
λ-MnO_2(P)	$Li_{1.01}Mn_{1.99}O_{4.12}$	8.06	0.100	0.28	$Li_{0.19}H_{0.23}Mn^{III}_{0.15}Mn^{IV}_{1.78}O_4$

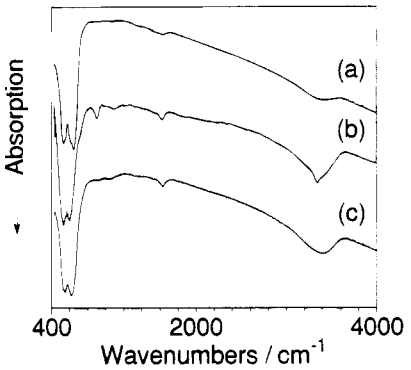

Figure 5. IR spectra of (a) lithium manganate prepared by method (C), (b) its acid-washed derivative λ-MnO_2(C), and (c) λ-MnO_2(C) after reinsertion of lithium in 0.1 M LiCl solution.

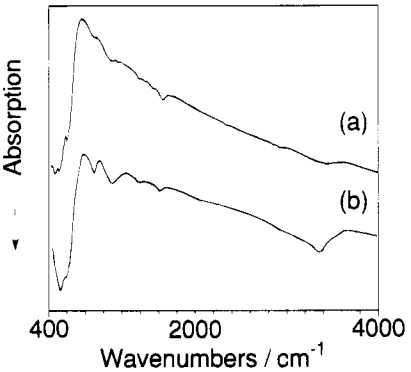

Figure 6. IR spectra of (a) λ-MnO_2(P) and (b) λ-MnO_2(G).

and some Mn^{III} present in the material. The continuous weight loss up to the transformation to Mn_2O_3 is reminiscent of that observed for λ-MnO_2(P), and suggests that there may be hydroxyl groups associated with Mn^{III} in both materials which were stable in the oxides up to 300 °C. The implications of these results in relation to the spectroscopic data will be discussed in the next section.

II. Spectroscopic Studies. *Infrared Absorption and Inelastic Neutron Scattering Spectra of the λ-MnO_2 Samples.* Infrared data have been reported for λ-MnO_2 materials in earlier studies,[11,19] but no serious attempts have yet been made to assign specific bands which are observed to be present in the acid washed materials but not in their lithiated precursors. However, infrared bands at 3430 and 920 cm^{-1} have been reported for λ-MnO_2 derived from parent spinels of composition close to $Li_{1.33}Mn^{IV}_{1.67}O_4$ and have been attributed[19] to a stretching vibration of a lattice hydroxyl group and a "lattice coupling vibration", respectively.

The infrared absorption spectra of powdered samples of the three lithium manganates, their corresponding lithium-extracted λ-MnO_2 materials, and of the λ-MnO_2 materials relithiated in LiCl solution, were recorded between 400 and 4000 cm^{-1} to follow changes in the spectra resulting from the ion-exchange process. Spectra after each reaction are shown for the preparation (C) in Figure 5, and the spectra for λ-MnO_2(G) and λ-MnO_2(P) are given in Figure 6. The spectra of the lithium-extracted λ-MnO_2 materials each show a band at 908 cm^{-1} which is not observed in either the lithium manganate precursors or the relithiated materials. This band is also markedly more intense for λ-MnO_2(C) and λ-MnO_2(G) than for λ-MnO_2(P), correlating with the

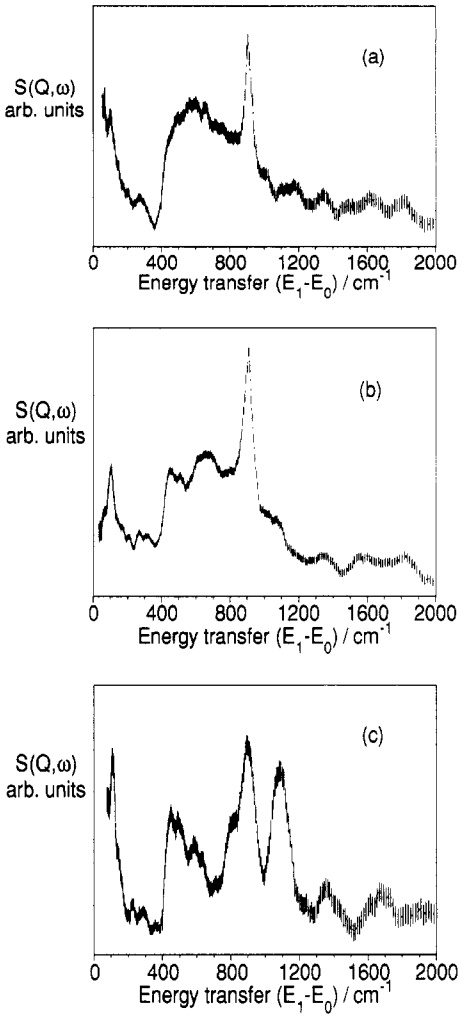

Figure 7. INS spectra of (a) λ-MnO_2(C), (b) λ-MnO_2(G), and (c) λ-MnO_2(P).

relative proton contents of the three materials. It is therefore, as noted previously, associated with proton insertion in the spinel lattice. Changes in the spectra between 1050 and 1090 cm^{-1} were also observed between lithium-extracted and lithiated samples but are difficult to interpret as a weak absorption was found in the lithium manganate precursors and relithiated materials as well as in the λ-MnO_2 samples. All the spectra show some water absorption between 1500 and 1700 cm^{-1} and above 3000 cm^{-1}. In the spectra of the proton-form spinels, these absorptions were observed at 1624 and 3345 cm^{-1}. Again, these absorptions were more intense for λ-MnO_2 (C) and λ-MnO_2 (G) than for λ-MnO_2 (P). Small changes were also observed in the manganese–oxygen vibrations between 400 and 700 cm^{-1} after lithium extraction and reinsertion.

While the infrared data permit the correlation of certain absorptions to the proton-form spinels, unambiguous assignment of the bands observed to specific vibrational modes could not be attempted on the basis of these data alone. For this reason the INS spectra of λ-MnO_2(C), λ-MnO_2(G), and λ-MnO_2(P) were recorded and those spectra are shown in Figure 7. INS spectroscopy gives vibrational data over an energy range comparable to the infrared but has the advantage that, in an oxide lattice, it is selective for vibrations involving displacement of hydrogen.

The dominant features between 800 and 1200 cm^{-1} in each of the INS spectra can be assigned to hydroxyl deformation modes. The intensity of an INS band is proportional to the amplitude of the normal coordinate associated with the vibration, and it has been established[29] that for hydroxylic systems the out-of-plane deformation mode, γOH, is the more intense. In the spectra of λ-MnO_2(C) and λ-MnO_2(G) the most intense signal is observed at 910 cm^{-1}. For λ-MnO_2(P) there are two principal features at 910 and 1080 cm^{-1} which are of approximately equal intensity to each other but of relatively lower intensity in relation to the 910 cm^{-1} signal found for λ-MnO_2(C) and (G). A good correlation of the position and relative intensity of the 910 cm^{-1} feature is therefore observed between infrared and neutron spectroscopies. On the other hand the feature at 1080 cm^{-1} was observed in INS for λ-MnO_2(P) only, despite the presence of broad and weak bands at this position in the infrared spectra of all three λ-MnO_2 materials. Some infrared absorption was also observed around 1080 cm^{-1} even in the parent lithium manganates and in the relithiated materials; therefore, this feature cannot be unambiguously assigned in infrared to a vibration associated with lattice protons. However the selectivity of INS spectroscopy for vibrations involving hydrogen confirms the presence of a hydroxyl deformation mode with this energy in λ-MnO_2(P). An alternative assignment of the 910 and 1080 cm^{-1} bands to out-of-plane and in-plane deformation modes of the same hydroxyl group, as described for example for proton-inserted VO_2[30] could be proposed. However it is preferred to assign these maxima as arising from γ-OH modes corresponding to two different hydrogen bonded hydroxyl groups since they are observed simultaneously for λ-MnO_2(P) only. The region around 900 cm^{-1} is also the high-wavenumber limit for the rocking and wagging modes of coordinated water. This is relevant to the existence of structural water in λ-MnO_2 (vide infra). However, our assignment to γ(OH) is maintained since hydroxyl groups are consistently present, even in conjunction with structural water.

The principal remaining features in the INS spectra include a strong lattice mode for all three samples at around 100 cm^{-1} and a series of overlapping peaks between 400 and 800 cm^{-1}. The correspondence of this range of energy to that of known infrared and Raman-active vibrations of [MnO_6] octahedra in spinel oxides, observed between 400 and 700 cm^{-1},[31] suggests that some of these modes may be activated in INS by riding motions of lattice protons in the λ-MnO_2 structure. However, librational modes of water molecules, typically observed in INS between 400 and 800 cm^{-1}, must be considered as the dominant contribution in this part of the spectra.

Variable-Temperature Studies. The infrared absorption spectra of powdered samples of the λ-MnO_2 materials were recorded over the temperature range from ambient to 220 °C. Changes were observed in the absorptions associated with the lattice protons, most significantly between 100 and 150 °C. The data for

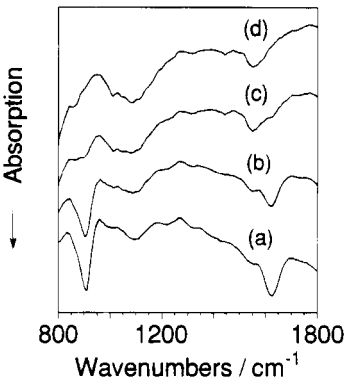

Figure 8. IR spectra of λ-MnO_2(C) at (a) 20, (b) 100, (c) 150, and (d) 220 °C.

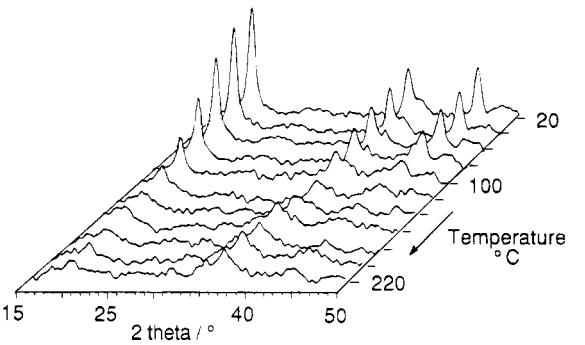

Figure 9. XRD patterns for λ-MnO_2(C) on heating at 20 °C increments from 20 to 220 °C.

λ-MnO_2(C), in the range 800−1800 cm^{-1}, are shown in Figure 8. The 908 cm^{-1} band is markedly influenced by heating, with a noticeable loss in its intensity even in the spectrum recorded at 100 °C. Above 100 °C this band is rapidly lost and is no longer present at 220 °C. Changes in intensity were also observed in the absorption at 1080 cm^{-1} but are difficult to interpret against a changing background. The loss of the lower 908 cm^{-1} mode can be correlated with the thermogravimetric data, where all of the lattice hydroxyls were observed to have been lost by 270 °C in λ-MnO_2(C) and λ-MnO_2-(G).

Simultaneously with the loss of the 908 cm^{-1} mode, changes in intensity were also observed in the bands due to water molecules. The spectra show clearly that these absorptions diminished in intensity concomitantly with that at 908 cm^{-1}. Through the course of a number of experiments, this association of the absorptions at 908, 1624, and 3345 cm^{-1} and identical behavior as a function of temperature was consistently found.

To identify the effects on the λ-MnO_2 spinel lattice resulting from the loss of the water and lattice hydroxyl observed in infrared spectroscopy, XRD patterns were recorded for λ-MnO_2(C) in an in situ heating experiment. These results are shown in Figure 9. The spinel reflections of the λ-MnO_2 phase are seen to decrease slightly in intensity on heating up to 100 °C and then to diminish rapidly, having almost completely disappeared by 150 °C. The destruction of spinel structure in the material therefore correlates with the loss of the lattice proton and water-associated modes in the infrared. As the temperature was increased, the XRD patterns show that the loss of the spinel structure gave rise to an almost amorphous phase which can be identified by at 300 °C as having some γ-MnO_2 struc-

(29) Howard, J.; Tomkinson, J.; Eckert, J.; Goldstone, J.; Taylor, A. D. *J. Chem. Phys.* **1983**, *78*, 3150.
(30) Chippendale, A. M.; Dickens, P. G.; Powell, A. V. *J. Solid State Chem.* **1991**, *93*, 526.
(31) Ishii, M.; Nakahira, M.; Yamanaka, T. *Solid State Commun.* **1972**, *11*, 209.

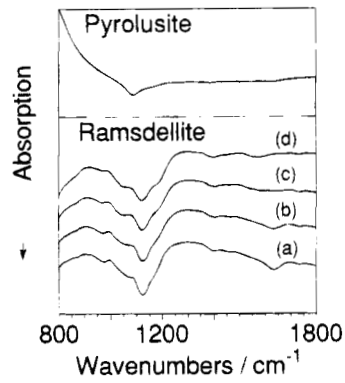

Figure 10. IR spectra of pyrolusite at 20 °C and ramsdellite at (a) 20, (b) 100, (c) 150, and (d) 220 °C.

ture. These results are therefore in disagreement with reports of a simple transformation of the λ-MnO_2 spinel to the pyrolusite β-MnO_2 structure at 270 °C.[19]

To better understand the vibrational data for the λ-MnO_2 materials, the infrared spectrum of pyrolusite (β-MnO2) was measured at room temperature and variable temperature spectra were measured for synthetic ramsdellite. These data are shown in Figure 10 for the range 800−1800 cm^{-1}. For pyrolusite, a single band appears in this part of the spectrum at 1090 cm^{-1}. In the case of synthetic ramsdellite, there are a number of overlapping bands centered around a room-temperature band maximum at 1125 cm^{-1}. The correlation of the positions of these infrared bands with those of signals attributed to inserted protons in the INS spectra of γ-MnO_2, an intergrowth of pyrolusite and ramsdellite structures, suggests that they could be attributed to hydroxyl deformation modes. Heating the synthetic ramsdellite sample to 150 °C resulted in complete loss of the infrared absorptions attributable to water molecules. However, for temperatures up to 220 °C, there are only small and gradual changes in the intensity of the envelope centered at 1125 cm^{-1}. This contrasts with the complete loss in intensity, over the same temperature interval, for the 908 cm^{-1} band in the λ-MnO_2 samples, and indicates that the proton sites giving lattice hydroxyl groups in ramsdellite MnO_2 are of much greater stability than the site corresponding to the 908 cm^{-1} hydroxyl deformation mode in the λ-MnO_2 structure.

Location of Inserted Protons in Manganese Dioxides. The bands observed in both the INS and infrared spectra of λ-MnO_2(C), λ-MnO_2(G), and λ-MnO_2(P) at 910 and 1080 cm^{-1}, and the infrared absorption bands of pyrolusite and synthetic ramsdellite centered at 1090 and 1125 cm^{-1}, are all assigned as deformation modes of hydroxyl groups. The features at 910 and 1080 cm^{-1} are similar in position to the bands observed in the INS spectra of chemically and electrochemically reduced γ-MnO_2, where they have been assigned[23,24] to "isolated" protons located in high symmetry sites, which are nearest-neighbor and next-nearest-neighbor to vacancies and to Mn^{III} ions, and with the hydrogen not covalently bound to lattice oxygen atoms. Such sites are considered to be similar to those of hydrogen in metal hydrides. Our assignments are at variance with these interpretations.

The lattice of γ-MnO_2 is described as an intergrowth of pyrolusite and ramsdellite structures, so that the similarity in the vibrational data for inserted protons

Table 3. Nearest Oxygen−Oxygen Distances (pm) for Manganese(IV) Oxides

		ramsdellite	
λ-MnO_2	pyrolusite	pyramidal oxygen[a]	planar oxygen[a]
255	246	242	251
255	267	242	271
255	267	251	271
285	267	273	271
285	267	273	271
285	267	277	273
285	267	277	273
285	267	285	277
285	267	285	277
314	287	301	285
314	287	301	285
314	318	321	321

[a] The crystallographic description of the ramsdellite structure defines two types of oxygen atom, each distinguished by the geometry of coordination to three manganese ions.[25]

in all of these manganese oxides is not unexpected. For each of the materials studied, oxygen−oxygen distances have been calculated from published atomic coordinates.[17,25] In each case, the oxygen atom lattice shows a range of values for the O- - -O distance, with interatomic separations as short as 242 pm in the case of ramsdellite. The nearest oxygen−oxygen distances for an ideal λ-MnO_2 lattice (containing no residual lithium and entirely Mn^{IV}), pyrolusite, and ramsdellite are listed in Table 3.

Correlations of the frequencies observed for γOH modes of a large range of compounds with crystallographically determined O- - -O distances of greater than 240 pm have shown[32] that, as R(O- - -O) increases, γOH decreases from a maximum frequency of approximately 1250 cm^{-1} down to around 900 cm^{-1} for weakly hydrogen-bonded systems. This range fits with the present INS and infrared data. Precisely calculated crystallographic O- - -O distances for an ideal MnO_2 structure should be considered as only approximations to the real structure surrounding localized hydrogen atom sites. It follows that any correlation between O- - -O distances determined by X-ray crystallography and vibrational frequency can only be of use in indicating a trend, rather than an absolute tool. The shortest O- - -O distance is found in ramsdellite, and this is the manganese oxide with the highest wavenumber γOH mode. Synthetic ramsdellite also displays both the greatest range of O- - -O distances and the most complex γOH band structure in the infrared. The observation of a γOH mode at the lower value of 910 cm^{-1} in the λ-MnO_2 materials implies that the hydrogen ion is associated with the longer O- - -O distances in the spinel structure.

A part of the unit cell of the spinel structure is shown in Figure 11. There are several possible positions for the proton in the spinel lattice. In the upper part of the figure, showing the geometry around an oxygen coordinated to three Mn ions and a tetrahedral vacancy, these positions are labeled i−iii and correspond to the three shortest O- - -O distances in Table 3. Position i, corresponding to the shortest O- - -O distance of 255 pm, places the proton along an edge shared between two occupied 16d octahedral sites, while position ii, relating to the O- - -O distance of 285 pm, places the proton between two oxygens along an edge of the [MnO_6]

(32) Novak, A. *Struct. Bonding* **1974**, *18*, 177.

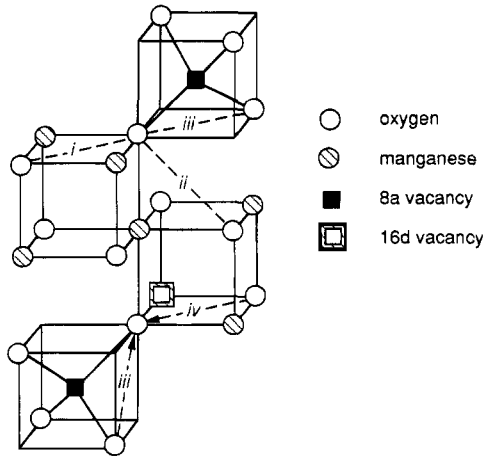

Figure 11. Section of the unit cell of λ-MnO_2 showing possible locations of inserted protons at positions i–iv. Arrows in the lower part of the diagram illustrate the possible association of two protons with the same oxygen to form coordinated water.

octahedron shared with vacant interstitial sites. Position iii associates the proton with the edge of a vacant 8a tetrahedral site previously occupied by lithium. At this stage we consider the position labeled iii to be the most likely to correspond to the 910 cm^{-1} feature observed in the IR and INS spectra of all three λ-MnO_2 samples. This position associates the proton with the tetrahedral sites vacated by lithium ions. Correlation of the 910 cm^{-1} mode with the 8a tetrahedral site is seen to be consistent with the disappearance of this mode in infrared spectroscopy in the same temperature range (100–150 °C) as the destruction of the spinel λ-MnO_2 lattice observed in XRD. Association of the proton with the position of the exchanged lithium ion does not however locate it symmetrically in the interior of the site. The location of the hydrogen atom between two oxygen atoms defining a tetrahedral edge would be accompanied by a local disorder in the oxygen lattice, but such a local perturbation is effectively masked by space-averaging of the oxygens in the overall presence of high symmetry sites in the lattice. Furthermore, vacancies in 16d octahedral sites and the presence of residual lithium in the λ-MnO_2 materials will give rise to additional local distortions in the structure.

The presence of protons associated with a γOH mode at 1080 cm^{-1} in the INS spectrum of λ-MnO_2(P) and therefore associated with a second site can be explained with reference to the pyrolusite and synthetic ramsdellite materials, and to INS spectra previously published for γ-MnO_2.[22-24] For these latter manganese dioxides, vibrational modes observed in the region of 1100 cm^{-1} are attributed to protons associated with Mn^{III} ions in the lattice. These protons are considered to be inserted in interstitial locations corresponding to vacant octahedral sites forming channels which run parallel to the chains of edge-sharing [MnO_6] octahedra in the pyrolusite and ramsdellite structures. Compositional and structural analyses of the λ-MnO_2 materials showed that λ-MnO_2(P) contained a significant proportion of Mn^{III}, whereas the manganese in λ-MnO_2(C) and (G), as in their precursors, was practically all Mn^{IV}. It was also noted, in thermogravimetry, that λ-MnO_2(P) was unique among the three λ-MnO_2 materials in showing further weight loss beyond 300 °C and up to the reduction to Mn_2O_3, which begins above 500 °C. The results were similar to those for the synthetic ramsdellite, for which it was found that the lattice hydroxyl modes at around 1100 cm^{-1} in the infrared were only slightly affected on heating up to the limit of the in situ experiments at 220 °C. These results are consistent with the assignment of the 1080 cm^{-1} mode in the INS spectrum of λ-MnO_2(P) to a hydroxyl group associated with Mn^{III} in the λ-MnO_2 lattice, at an octahedral site having greater thermal stability than the tetrahedral site to which the 910 cm^{-1} mode is correlated. With reference to Figure 11, this second proton site might be identified with position ii when the neighboring octahedron is occupied by Mn^{III}. A proton at such a site in the spinel structure could then be expected to have similarities with protons inserted in γ-MnO_2 by chemical or electrochemical reduction if, in both structures, the protons are considered to be covalently bonded to oxygen coordinating a Mn^{III} ion.

Structural Water in λ-MnO_2. The observation of a single dominant γOH mode at 910 cm^{-1} in the INS spectra of λ-MnO_2(C) and λ-MnO_2(G) implies that only hydroxyl groups associated with tetrahedral sites were present in these samples. Complete lithium extraction from lithium manganates of composition close to $Li_{1.33}Mn_{1.67}O_4$ leaves vacancies in both tetrahedral 8a sites and approximately one sixth of the octahedral 16d sites (those occupied by lithium in the precursor), giving a λ-MnO_2 structure which would be expected to be stabilized by chemically bonded protons associated with both sites and therefore to give rise to two corresponding γOH modes. However, in the variable temperature IR studies, the observation of an association between bands due to water molecules and the 910 cm^{-1} hydroxyl mode suggests that lattice water may play a role in stabilizing the protonated form of λ-MnO_2. The spectral modifications observed below 150 °C, which include the loss of the water bands, are difficult to explain as being due solely to the condensation of lattice hydroxyl groups. The drastic structural changes associated with the loss of these bands further supports their assignment to the presence of water performing a structural role in λ-MnO_2.

The possibility of the existence of water molecules in the λ-MnO_2 lattice may be explained with reference to the coordination of an oxygen associated simultaneously with both a 8a tetrahedral vacancy and a 16d octahedral vacancy. For λ-MnO_2 derived from $Li_{1.33}Mn_{1.67}O_4$, one sixth of the oxygens in the lattice have this coordination. As illustrated in the lower part of Figure 11, this gives rise to another possible position iv for a lattice proton, corresponding to position i above but now located at a vacant 16d site. If a proton located in position iv and a second proton at the tetrahedral vacancy in position iii associated with the same oxygen at the common apex, this would effectively give a molecule of water at the corner shared between the vacant 8a tetrahedron and 16d octahedron. Such a pattern of association, distributed through the λ-MnO_2 structure, might give an overall equilibrium between coordinated water molecules and lattice hydroxyl groups associated with 8a sites.

The similarities and differences between the structural water thus proposed for λ-MnO_2 and that in γ-MnO_2 and ramsdellite can now be considered. In these latter materials, the presence of structural water

has been recognised as essential to the electrochemical activity. Ruetschi[33-35] has proposed that while γ-MnO_2 will contain a small portion of protons associated with Mn^{III} defects, the major part of the structural water may be accounted for by hydroxyl groups coordinating octahedral Mn^{IV} vacancies. There are four such Ruetschi protons for each Mn^{IV} vacancy in γ-MnO_2, localized at the vacancy sites at room temperature. This "structural water" is removed between 150 and 400 °C due to progressive annealing of the Mn vacancies and is visualized as a diffusion of the associated protons to the surface of the crystal where they combine with surplus O^{2-} to evaporate as water.

Although the protons associated with octahedral vacancies in λ-MnO_2 bear some conceptual resemblance to the Ruetschi protons in γ-MnO_2, important differences are observed. First, the overall "water" content of protonated λ-MnO_2 derived from $Li_{1.33}Mn_{1.67}O_4$ is much higher than that of γ-MnO_2. A typical γ-MnO_2 contains around 6% octahedral vacancies,[33] and therefore has a chemical formula that can be written

$$Mn_{(1-x)}O_{(2-4x)}(OH)_{4x} \qquad x = 0.06$$

or

$$MnO_2{\cdot}2xH_2O \qquad x = 0.06$$

For λ-MnO_2 prepared by complete ion exchange of $Li_{1.33}Mn_{1.67}O_4$, the chemical formula is:

$$H_{1.33}Mn_{1.67}O_4$$

which may be written alternatively as

$$MnO_{1.6}(OH)_{0.8}$$

or

$$MnO_2{\cdot}0.4H_2O$$

λ-MnO_2 may therefore contain up to 4 times the quantity of "lattice water" typically observed for γ-MnO_2.

Second, the Ruetschi protons in γ-MnO_2 are considered to be present in the lattice uniquely as forming OH^- ions. On the contrary, the spectroscopic data for λ-MnO_2 shows that a significant portion of the inserted protons give identifiable coordinated water species which are assumed to be present at the intersections of adjacent octahedral and tetrahedral vacancies. The third essential difference is that the structural water in λ-MnO_2 is apparently lost at much lower temperatures than in γ-MnO_2, suggesting that a different mechanism may be involved. For γ-MnO_2 the activation energy of water removal is supposed to be determined by the activation energy of manganese (vacancy) diffusion, which commences at around 150 °C. The much higher proportion of cation vacancies in λ-MnO_2 (due to extracted lithium) may account for a smaller lattice binding energy and easier removal of the structural water. However it is difficult to believe that the almost complete destruction of the λ-MnO_2 crystal structure between 80 and 150 °C which accompanies the removal of the lattice water could be activated by the diffusion of Mn ions at such low temperature. It must be concluded that the coordination of water molecules is important in stabilizing the λ-MnO_2 structure. The continuing mass loss above 150 °C observed in the thermal analyses of the λ-MnO_2 materials is then probably due to a process similar to that in γ-MnO_2, where remaining protons are lost in the annealing of manganese vacancies. The protons remaining in the materials after the low-temperature destruction of the λ-MnO_2 phase would be expected to conform to the dynamics of protonated γ-MnO_2. These protons are more difficult to observe in IR spectroscopy than the characteristic λ-MnO_2 protons absorbing at 908 cm^{-1} but are expected to contribute to the absorptions observed (most strongly for the synthetic ramsdellite) around 1100 cm^{-1}.

Conclusion

The observed chemical analytical, thermogravimetric, X-ray diffraction, infrared, and neutron scattering data for λ-MnO_2 can, therefore, be interpreted in terms of a conventional manganese oxide lattice. Furthermore, and as is usually found in any structural or spectroscopic study of a solid protonic system,[36] the inserted protons interact strongly with the local environment such that, in the case of λ-MnO_2, lattice hydroxyl, or water groups are formed. This interpretation for λ-MnO_2 is at variance with that proposed for hydrogen-inserted γ-MnO_2[22-24] since it is without recourse to a model invoking "isolated hydrogen ions". Hydroxyl groups and structural water molecules are local defects in the spinel lattice, and their dynamics are governed by the local geometry of nearest neighbor oxygens, their influence on crystal symmetry being space-averaged. Our studies continue on the specific lithium ion-exchange properties of λ-MnO_2, in particular when highly dispersed in xerogel matrixes.

Acknowledgment. B.A. gratefully acknowledges the financial assistance of the French Ministère des Affaires Etrangères through the France-New Zealand Cultural Exchange, and also grants from the Royal Society of New Zealand and the Internal Grants Committee of Victoria University of Wellington. E.P.S.R.C. is thanked for access to the neutron facility at ISIS.

CM950235N

(33) Ruetschi, P. *J. Electrochem. Soc.* **1984**, *131*, 2737.
(34) Ruetschi, P. *J. Electrochem. Soc.* **1988**, *135*, 2657.
(35) Ruetschi, P. J.; Giovanoli, R. *J. Electrochem. Soc.* **1988**, *135*, 2663.

(36) (a) Thomas, J. O. In *Proton Conductors*; Colomban, P., Ed.; Cambridge University Press: Cambridge, 1992; p 79. (b) Jones, D. J.; Rozière, J. *Ibid.*, p18.